

Crystal structure of a 12 ANK repeat stack from human ankyrinR

Peter Michaely¹, Diana R. Tomchick²,
Mischa Machius² and
Richard G.W. Anderson

Departments of Cell Biology and ²Biochemistry, University of Texas Southwestern Medical Center, Dallas, TX 75235-9039, USA

¹Corresponding author
e-mail: peter.michaely@utsouthwestern.edu

Ankyrins are multifunctional adaptors that link specific proteins to the membrane-associated, spectrin-actin cytoskeleton. The N-terminal, ‘membrane-binding’ domain of ankyrins contains 24 ANK repeats and mediates most binding activities. Repeats 13–24 are especially active, with known sites of interaction for the Na/K ATPase, Cl/HCO₃ anion exchanger, voltage-gated sodium channel, clathrin heavy chain and L1 family cell adhesion molecules. Here we report the crystal structure of a human ankyrinR construct containing ANK repeats 13–24 and a portion of the spectrin-binding domain. The ANK repeats are observed to form a contiguous spiral stack with which the spectrin-binding domain fragment associates as an extended strand. The structural information has been used to construct models of all 24 repeats of the membrane-binding domain as well as the interactions of the repeats with the Cl/HCO₃ anion exchanger and clathrin. These models, together with available binding studies, suggest that ion transporters such as the anion exchanger associate in a large central cavity formed by the ANK repeat spiral, while clathrin and cell adhesion molecules associate with specific regions outside this cavity.

Keywords: anion exchanger/ANK/ankyrin/clathrin/spectrin

Introduction

Ankyrins are protein adaptors that bridge between the spectrin-actin cytoskeleton and proteins involved in ion transport, cell adhesion and membrane trafficking. Linkages with ion transporters represent the largest class and include associations with the Cl/HCO₃ anion exchanger, the Na/Ca exchanger, Na/K ATPase, IP₃ receptor, ryanodine receptor and voltage-gated Na channels (Bennett and Stenbuck, 1979; Nelson and Veshnock, 1987; Srinivasan *et al.*, 1988; Joseph and Samanta, 1993; Li *et al.*, 1993; Bourguignon *et al.*, 1995; Festy *et al.*, 2001). These linkages serve to anchor the spectrin-actin cytoskeleton on the membrane and to concentrate these transporters in specialized membrane domains (reviewed in Bennett and Baines, 2001). The ankyrin linkages with cell adhesion

molecules such as the L1 family (Davis *et al.*, 1993) enhance cell adhesion and facilitate the incorporation of cells into tissues (Hortsch *et al.*, 1998; More *et al.*, 2001). Ankyrins also bind clathrin and participate in membrane trafficking at the level of both coated pit budding (Michaely *et al.*, 1999) and trafficking of specific membrane proteins (Tuvia *et al.*, 1999).

Metazoan cells employ a large number of ankyrin isoforms for these different functions. Vertebrates have three ankyrin genes (*ank1–3*) that code for three families of proteins (ankyrinR, B and G, respectively). Most ankyrin isoforms contain two conserved domains that mediate protein-protein interactions. A central, ‘spectrin-binding’ domain associates with β -spectrin, while the N-terminal, ‘membrane-binding’ domain binds most other proteins. Isoform specificity is determined by the variably spliced C-terminal domain, which contains isoform-specific targeting information and regulatory functions that modulate the binding activities of the two protein interaction domains (reviewed in Bennett and Baines, 2001).

Of fundamental importance to ankyrin function is the extraordinary ability of the membrane-binding domain to bind many unrelated proteins. This region is highly conserved and consists of 24 copies of the ANK repeat motif (also referred to as ankyrin repeats). ANK repeats are a common motif whose L-shaped structure consists of two α -helices and a long loop. Typically, repeats stack in a linear fashion to form curved assemblies that contain between four and seven repeats and associate with a single protein target (reviewed in Sedgwick and Smerdon, 1999). Ankyrins, in contrast, contain 24 repeats that interact with at least 10 distinct proteins. Proteolytic mapping suggests that the 24 repeats are divided into four smaller domains (D1, D2, D3 and D4) of six repeats each; however, it is not clear how these subdivisions relate to protein associations since many binding sites overlap the domain boundaries (Michaely and Bennett, 1993, 1995b).

Herein, we have determined the crystal structure of the D34 region of human ankyrinR, which consists of repeats 13–24 and a small portion of the spectrin-binding domain. We find that the 12 ANK repeats in D34 are stacked in the form of a contiguous, left-handed superhelix. The spectrin-binding domain segment is extended and interacts with the repeat stack in a peptide-in-groove association. The structural information has been used to model the 24 repeats of the entire membrane-binding domain and the associations of the D34 region with the clathrin heavy chain and the Cl/HCO₃ anion exchanger. We propose that the membrane-binding domain forms a large, spiral, hook-like structure. Ion transport proteins such as the anion exchanger may associate with the concave surface of this hook, while clathrin and cell adhesion molecules decorate the outside of the helical hook.

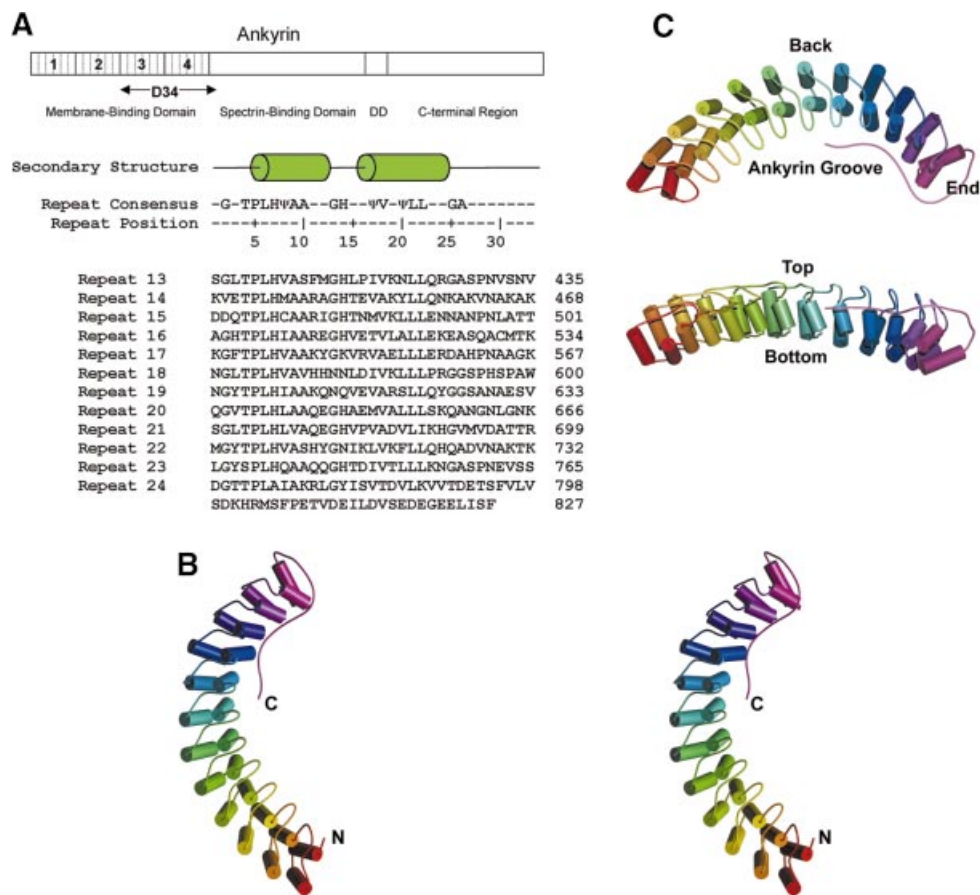


Fig. 1. Structure of the D34 region of ankyrinR. (A) Ankyrins typically are composed of four domains: an ANK repeat bearing, ‘membrane-binding’ domain, a central ‘spectrin-binding’ domain, a death domain (DD) and a C-terminal regulatory domain. The D34 region of ankyrinR contains ANK repeats 13–24 and a short portion of the spectrin-binding domain. Cylinders indicate the positions of the two helical segments in each repeat. Amino acids are given as one-letter code, where Ψ indicates a non-polar residue. Position numbering within repeats is based upon the exon–intron boundaries of the *ank1* gene. The amino acid sequence of the D34 region is shown, with the repeat designation on the left and the amino acid number on the right of the sequence block. (B) Stereo view of D34. Individual repeats are rainbow colored such that repeat 13 is red and repeat 24 is violet. (C) Surface labels are given for the repeat stack. The bottom image is rotated 90° relative to the top image.

Results

Several regions of the membrane-binding domain of human ankyrinR were utilized in crystallization attempts. As has been seen in other ANK repeat proteins (Michel *et al.*, 2001), both the membrane-binding domain and the proteolytically defined subdomains were prone to aggregation. Inclusion of residues 798–827 from the spectrin-binding domain markedly improved protein solubility. Crystallization efforts therefore concentrated on constructs bearing residues 1–827 (D1234), 402–827 (D34) and 600–827 (D4) (Figure 1A). Small, poorly diffracting crystals were obtained initially with the D34 construct. Re-engineering of the D34 construct to include six glycine residues at the N-terminus improved protein solubility and crystal quality. Optimization of the crystallization conditions generated large crystals that exhibited the symmetry of space group $P6_322$ with one molecule per asymmetric unit. The crystal structure was solved by the multi-wavelength anomalous dispersion (MAD) method using a seleno-methionine (SeMet) variant of D34 (Table I). The final refined model of the native protein contains residues 405–797 and 802–812 of human ankyrinR (Table I).

Structure of D34

The structure of D34 (Figure 1B and C) consists of a contiguous stack of 12 ANK repeats (repeats 13–24 of the membrane-binding domain) plus a short extended segment from the start of the spectrin-binding domain. Individual ANK repeats have the typical ‘L’-shaped structure seen in ANK repeats from non-ankyrin proteins (Sedgwick and Smerdon, 1999). The ‘L’ structure consists of two short, antiparallel α -helices (positions 4–11 and 15–23 of the ANK repeat consensus sequence) followed by a long loop (positions 24–30). Individual repeats are linked by a β -hairpin that contains amino acids at positions 31–33 from one repeat and positions 1–3 of the next repeat (Figure 2A). The repeats generate a linear stack such that the α -helices of adjacent repeats form a four-helical bundle (Figure 2B). The long loop covers one end of the helical bundle, while the β -hairpin extends away from the bundle, perpendicular to the axis of the first helix and the repeat stack. At the C-terminus of the repeat stack, the spectrin-binding domain segment adopts an extended conformation that folds back and binds in a cleft formed by repeats 20–24.

Table I. Data collection, structure determination and refinement

Data collection			
Crystal	Native	SeMet	SeMet
Energy (eV)	12 661.1	12 659 (peak)	12 658.7 (inflection)
Resolution range (Å)	50.0–2.50	99.0–2.79	99.0–2.79
Total observations	415 031	409 137	220 227
Unique reflections	37 994	25 576	24 337
Data completeness (%)	98.4 (93)	89.9 (44.2)	85.2 (35)
R_{merge} (%) ^a	8.2 (69.9)	9.1 (57.9)	8.4 (70)
$I/\sigma(I)$	22.6 (1.3)	29.4 (1.7)	21.3 (1.6)
Phase determination			
Anomalous scatterer	8 Se sites		
Figure of merit (acentric/centric/overall)	0.256/0.171/0.243		
Refinement statistics			
Resolution range (Å)	30.0–2.70		
Wilson B -factor (Å ²)	67		
No. of reflections $R_{\text{work}}/R_{\text{free}}$	29 145/1155		
Atoms (non-H protein/halide)	3085/10		
R_{work} (%)	31.9		
R_{free} (%) ^b	30.3		
R.m.s.d. bond length (Å)	0.01		
R.m.s.d. bond angle (°)	1.62		
Mean B -value (Å ²) (main chain/side chain/halide)	113.8/114.4/129.3		
Cross-validated σ_A -coordinate error (Å)	1.07		
Missing residues	4 (798–801)		
No. of alternative conformations	3		

Data for the outermost shell are given in parentheses.

^a $R_{\text{merge}} = 100 \sum_h \sum_i |I_{h,i} - \langle I_h \rangle| / \sum_h \sum_i I_{h,i}$, where the outer sum (h) is over the unique reflections and the inner sum (i) is over the set of independent observations of each unique reflection.

^b R_{free} is calculated for a randomly selected 3.7%.

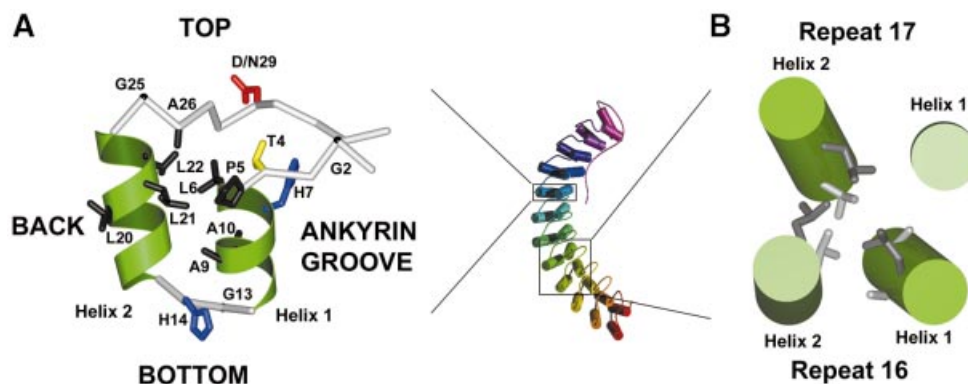


Fig. 2. Consensus residues of the ANK repeat. (A) The conformation of conserved residues of the ANK repeat consensus sequence is shown, oriented along the axis of the repeat stack. The α -helical segments are depicted as ribbons (green), and the non-helical segments are depicted as a C_α trace (light gray). Conserved histidines are blue, aspartates and asparagines are red, threonines are yellow, and aliphatic residues are black. Each repeat has four solvent-exposed surfaces as indicated. (B) The helical bundle core between repeats 16 and 17 is shown. Shown in light gray are Ala510, Ala511, Val519 and Val551 at positions 9, 10 and 18 of repeat 16 and position 17 of repeat 17, respectively. These residues are situated below the dark gray shaded Leu507, Leu523 and Leu555 at positions 6 and 22 of repeat 16 and position 21 of repeat 17, respectively. An image of the D34 structure is given between the panels for reference.

The repeat stack

All repeats within D34 have 33 amino acids and show strong homology with the consensus sequence, -G-TPLHΨAA--GH--ΨV-ΨLL--GA--D/N---, where Ψ designates aliphatic residues. Table II and Figure 2B summarize how the consensus residues define the boundaries of the two helices, stabilize the conformation of individual repeats and form the interfaces between repeats.

The threonine at position 4 of the consensus sequence (Thr[4], Pro[5], Gly[13], Gly[25] and Ala[26]) determine the boundaries of the helices. Thr[4] is the N-terminal capping residue of the first helix and frequently forms a hydrogen bond with the backbone amide of the third residue of the helix. Pro[5] starts the first helix most probably because its dihedral angle (ϕ) is restricted by the proline ring to a value near the optimal ϕ for helices

Table II. Selected non-core contacts

Intra-repeat interactions							
Position	Common residue	Atoms	↔	Position	Common residue	Atoms	Contact type
4	Thr	sc		7	His	sc	H-bond
4	Thr	sc		7	His	N	H-bond
7	His	sc		30	Non-polar	O	H-bond
27	Polar	sc		28/29	Varies	mc	H-bond
Inter-repeat interactions outside the hydrophobic core							
Repeat <i>n</i>				Repeat <i>n</i> + 1			
Position	Common residue	Atoms	↔	Position	Common residue	Atoms	Contact type
7	His	sc		3	Varies	O	H-bond
11	Varies	mc		8	Non-polar	sc	vdW
10/11	Varies	O		14	His	sc	H-bond
18/22	Non-polar	mc		20	Non-polar	sc	vdW
28	Non-polar	sc		26	Ala	sc	vdW
29	Asx	sc		27	Polar	N	H-bond
32	Varies	O		2	Varies	N	H-bond
32	Varies	N		3	Varies	O	H-bond
33	Varies	N		1	Varies	O	H-bond

Contacts of the hydrophobic cores of helical bundles have been excluded; see Figure 2B.

vdW, van der Waals contact; H-bond, hydrogen bond contact; sc, side chain; mc, main chain; O, carbonyl oxygen; N, amide nitrogen.



Fig. 3. Spectrin-binding domain fragment. Shown is a stereo pair of the interaction between residues 802–812 and the repeat stack. Residues 802–812 are shown as sticks on the ankyrin groove surface of repeats 19–24. Atoms are colored gray for carbon, red for oxygen, blue for nitrogen and green for sulfur. The displayed surface is colored by electrostatic potential from -10 kT (red) to $+10$ kT (blue). The electrostatic surface potential was calculated and rendered in the program GRASP (Nicholls *et al.*, 1991).

(Aurora and Rose, 1998; Richardson and Richardson, 1988). Gly[25] and Ala[26] constitute a common C-terminal helix cap (Edwards *et al.*, 1987). Glycines generally are considered to be helix-disrupting residues and Gly[13] most probably promotes the formation of the short loop that connects the first and second helices.

Residues at positions 9, 16, 24, 27 and 30 appear to stabilize the fold of individual repeats. Positions 16 and 24 frequently contain negative and positive charges, respectively, and probably serve to stabilize the second helix by neutralizing its dipole moment (Shoemaker *et al.*, 1987). Ala[9] and hydrophobic residues at position 30 appear to help orient the two helices relative to each other. Position 27 stabilizes the unusual conformation of the long loop that separates the second helix from the β -hairpin by forming a hydrogen bond to the backbone amide of position 29.

Residues at many conserved positions form the inter-repeat contacts that join adjacent repeats to the repeat

stack. The contacts made by these positions can be classified into three groups. Centermost are the van der Waals contacts made by residues that form the hydrophobic core of the four-helix bundles. These residues include Leu[6], Ala[10], Leu[21], Leu[22] and mid-sized hydrophobic residues at positions 17 and 18 (Figure 2B). A second layer of van der Waals contacts made by hydrophobic residues at positions 8, 20, 26 and 28 surrounds this central core (Table II). Finally, an outer layer of hydrogen bonds formed by His[7], His[14], Asn/Asp[29] and residues of the β -hairpin provide additional inter-repeat connections (Table II).

The 12 ANK repeats in D34 stack side by side to form a 125 Å long, left-handed superhelix (Figure 1B). Each repeat is twisted counter-clockwise $2-3^\circ$ relative to the preceding repeat and contributes 13° of pitch to the superhelix. Equivalent residues in each repeat of the superhelix form four distinct surfaces on the repeat stack. These surfaces consist of (i) a concave ‘bottom’ surface using

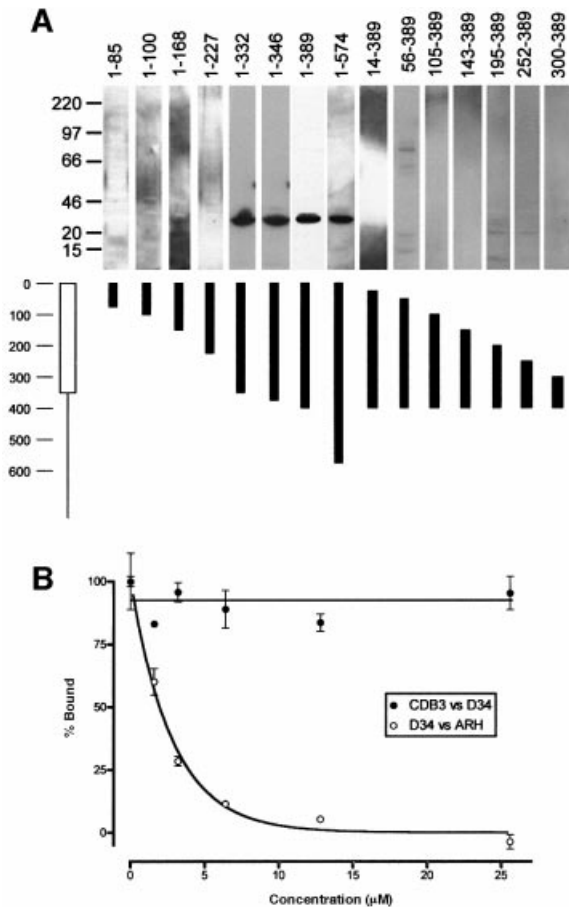


Fig. 4. Binding site mapping. (A) The upper portion presents far-western blots (see Materials and methods) showing the relative ability of GST fusions with clathrin fragments to associate with the D4 region. The numbers above each lane indicate the amino acids of clathrin present in each fusion. The lower portion of the panel provides a pictorial representation of these regions. On the left is an amino acid marker together with a diagram indicating the location of the β -propeller (box) and α -helical (line) segments of the CTD. (B) *In vitro* binding assays were performed using 50 nM ^{125}I -labeled CTD1–494, D34- (closed circles) or ARH- (open circles) coupled Sepharose beads, and increasing concentrations of CDB3 (closed circles) or D34 (open circles). ARH (autosomal recessive hypercholesterolemia protein) contains a canonical clathrin box sequence, while the D34 region does not. All assays were carried out in triplicate with standard error shown with error bars. Values shown represent specific binding only.

residues at positions 13–16; (ii) a concave ‘ankyrin groove’ surface (Sedgwick and Smerdon, 1999) using positions 1, 3, 11, 12 and 32; (iii) a convex ‘back’ surface comprising positions 19, 23 and 24; and (iv) a broad, convex ‘top’ surface consisting of positions 27, 29, 31 and 33 (Figures 1C and 2A). The ankyrin groove surface is directed towards the axis of the superhelix, while the junction between the top and back surfaces is directed away from this axis. Residues that form these surfaces are solvent exposed and are in variable positions of the consensus sequence. The first and last repeats have additional ‘end’ surfaces that contain hydrophilic residues at consensus positions that are typically hydrophobic and protected from solvent in the helical bundles of the inner repeats.

Residues in the helical bundle cores control the superhelical curvature of the repeat stack. The ankyrin

groove exhibits concave curvature because the helices of the inner row, consisting of the first helices in successive repeats, pack more tightly than the helices in the second, outer row. The packing difference is due largely to residues at positions 10, 17 and 18. The small side chains of residues at position 10 allow the first helices to pack closer than the mid-sized residues at positions 17 and 18 in the second helices (Figures 1C and 2). The curvature about the bottom surface is due to equivalent positions in successive repeats being farther apart near the top surface than at the bottom surface. The shorter spacing at the bottom is determined by the relatively small side chains of residues at positions 10, 17 and 18 as compared with the larger leucines at positions 6, 21 and 22 at the top (Figures 1C and 2).

ANK repeat interactions

In the D34 structure, the ankyrin groove surface of repeats 20–24 associates with the first 11 residues of the spectrin-binding domain. This 11 residue segment binds in an extended conformation, antiparallel to the repeat stack (Figures 1B and 3). The interaction is mediated by a number of van der Waals contacts involving His802, Met804, Pro807 and Val810, as well as polar interactions involving Ser805, Glu808 and Asp811. Ser805 plays a central role, forming both main chain and side chain hydrogen bonds with Tyr702, Gln740 and Gln743 on the repeat stack.

The D34 region of ankyrins associates with at least five proteins: the clathrin heavy chain, the Cl/HCO₃ anion exchanger, Na/K ATPase, the L1 family of cell adhesion molecules and sodium channels of the voltage-gated and amiloride-sensitive family (Srinivasan *et al.*, 1992; Michaely and Bennett, 1995a,b; Thevananther *et al.*, 1998; Michaely *et al.*, 1999). These proteins do not share sequence homology and, therefore, do not use a common motif for D34 binding. In the following, we have focused on the associations with clathrin and the Cl/HCO₃ anion exchanger (band 3), because structural information exists for the ankyrin-binding regions of these two proteins (ter Haar *et al.*, 1998; Zhang *et al.*, 2000).

The association of D34 with the cytoplasmic domain of the anion exchanger (CDB3) is well characterized. Antibody competition and protein chimera studies indicate that the interaction surface on CDB3 involves residues 1–75, 118–141, 155–160 and 174–193 (Davis *et al.*, 1989; Willardson *et al.*, 1989). These residues form a slightly convex surface on the CDB3 dimer, which folds as a seven-stranded α/β sandwich and dimerizes by means of a shared α -helical motif (Zhang *et al.*, 2000). Both repeats 13–18 and 22–23 of D34 are required for binding to CDB3 (Davis *et al.*, 1991; Michaely and Bennett, 1995a).

The ankyrin interaction with clathrin is less well characterized. Previously, we identified an interaction between repeats 19–24 of ankyrin (D4) and the N-terminal domain of clathrin heavy chain (CTD) (Michaely *et al.*, 1999). The CTD contains a β -propeller-like arrangement of seven β -sheets followed by an extended series of α -helices. To map the ankyrin-binding site better on the CTD, we expressed various truncated forms of the CTD and tested their ability to interact with D4 using a far-western assay system (Davis *et al.*, 1991; Michaely and Bennett, 1993) (Figure 4A). The entire β -propeller region

(residues 1–332) of the CTD was required to interact with D4. Removing as few as 14 amino acids from the N-terminus was sufficient to abolish binding. Deletion of residues from either terminus disrupts the final β -sheet and may also affect the normal organization of the β -propeller.

Clathrin also binds proteins that contain the clathrin box sequence, LL(D/N)L(D/E), via a cleft on the β -propeller between the first and second β -sheets. To determine whether D34 binds near this region, we tested the ability of D34 to inhibit CTD binding to the clathrin box containing autosomal recessive hypercholesterolemia protein (ARH). Figure 4B shows that D34 is a good competitive inhibitor of CTD binding to ARH. In contrast, CDB3 did not compete with CTD for D34 binding. These results suggest that the D34-binding site on clathrin is near the first and last β -sheet of the β -propeller, while the clathrin-binding site on D34 involves repeats 19–24.

We used a protein-docking program suite, 3D-Dock, to model the interactions of the D34 region with CDB3 and the β -propeller of clathrin (Gabb *et al.*, 1997). Potential docking modes were identified based upon surface and charge complementarity. Probable models were then checked against steric and biochemical criteria. The model with the highest score for the clathrin association is shown in Figure 5A. The proposed contact is between

the first and last β -sheets of the CTD and the top surface of the last three repeats of D34. The interface shows a high degree of charge complementarity consistent with the observation that the interaction is sensitive to salt. We used a similar approach to look at potential interactions between D34 and CDB3. The modeling suggests that bottom and ankyrin groove surfaces of the ANK repeat stack associate with the CDB3 dimer on the surface opposite the dimer interface (Figure 5B). The proposed contact surface on CDB3 consists of the third helix and the loops that connect the first and second β -strands, the fifth β -strand and the second helix, the sixth and seventh β -strands, the sixth helix and the eighth β -strand, and the ninth and tenth β -strands. This interaction surface buries $>1500 \text{ \AA}^2$ and contains few potential salt bridges, which is in agreement with a high affinity interaction between D34 and CDB3 that is not salt sensitive (Michaely and Bennett, 1995a).

Modeling of the ankyrinR membrane-binding domain

In addition to interactions made by repeats 13–24 of the D34 region, several associations are known to require repeats 1–12. We have modeled the entire set of 24 repeats by extending the D34 superhelix to include all 24 ANK repeats, retaining the 13° pitch for each repeat. The model predicts that the entire membrane-binding domain forms a superhelical spiral with an axial length of 132 \AA and radius of 45 \AA (Figure 6A). The 800 residues of the full repeat stack provide a surface area of $>27\,000 \text{ \AA}^2$ for protein interactions. The wide spiral of the modeled membrane-binding domain has a more globular structure than the D34 construct, consistent with previously published hydrodynamic measurements (Michaely and Bennett, 1993). One interaction made by repeats 7–12 (D2) is an association with a second CDB3 dimer (Michaely and Bennett, 1995a). In Figure 6B, we extended the D34–CDB3 model to encompass all 24 repeats of the membrane-binding domain and both dimers of the CDB3 tetramer. Significantly, the combined model positions the D2 region so that it can associate with the second CDB3 dimer in the tetramer. The D2 association is salt sensitive, and the modeled association between D2 and the second CDB3 dimer includes several potential salt bridges.

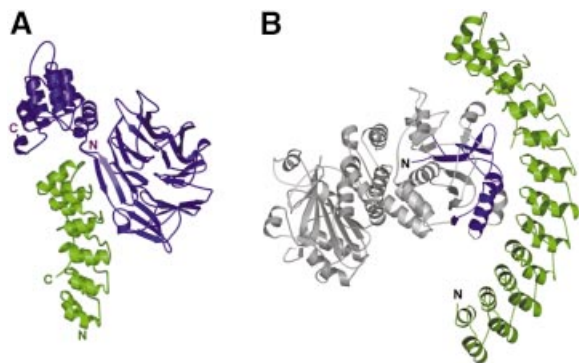


Fig. 5. Modeled binding partners. (A) The model for the complex of repeats 19–24 of D34 (green) with the CTD (purple). (B) The association of D34 (green) with the CDB3 dimer (gray and purple). Residues predicted to bind ankyrin are shown on CDB3 in purple.



Fig. 6. Membrane-binding domain. (A) A stereo view of a model of the membrane-binding domain viewed along the spiral axis with the C-terminus closest to the viewer. Repeats are rainbow colored such that repeat 1 is red and repeat 24 is violet. (B) An extension of the D34–CDB3 model to include all 24 repeats of the membrane-binding domain and all four subunits of the CDB3 tetramer. The membrane-binding domain is shown as a green ribbon, while the four subunits of the tetramer are shown as red, blue, cyan and pink ribbons. The D34 region of the membrane-binding domain interacts with the red subunit.

Discussion

We have determined the crystal structure of ANK repeats 13–24 and a small portion of the spectrin-binding domain of human ankyrinR. The 11 amino acid portion of the spectrin-binding domain binds through a peptide-in-groove interaction with the C-terminal ANK repeats. ANK repeats provide the principle sites of protein interaction on ankyrins, and we modeled the interactions of D34 with the clathrin heavy chain and CDB3. In D34, the individual ANK repeats adopt the typical 'L'-shaped conformation similar to that observed in structures of ANK repeats found in non-ankyrin proteins (reviewed in Sedgwick and Smerdon, 1999). Models based upon biochemical and hydrodynamic data had suggested that the 12 ANK repeats of the D34 region of ankyrinR were divided into two subdomains of six repeats each. The D34 structure now reveals that these 12 ANK repeats form a contiguous extended stack that provides an extensive surface area for protein interactions.

A striking feature of the ANK repeats in ankyrinR is their uniformity in both amino acid sequence and three-dimensional structure. Most repeats in ankyrins and all repeats in the D34 region consist of exactly 33 amino acids with strong adherence to the consensus sequence. Because most consensus residues provide inter-repeat contacts, the strong conservation with the repeat consensus sequence results in extensive and uniform connectivity between repeats (Figures 1 and 2; Table II). Extensive connectivity may be required for ankyrins to fulfill their role as the primary linker protein between the spectrin–actin cytoskeleton and membranes. Mechanical deformations of cells and tissues most probably place stress on this linkage. The abundance of inter-repeat contacts may protect the repeat stack from mechanical unfolding. In addition, the uniform nature of the inter-repeat contacts may allow differential splicing to remove individual repeats without compromising the integrity of the repeat stack. All ANK repeat-encoding exons of vertebrate ankyrins have either one or two repeats with exon boundaries exactly in register with position one of the repeat consensus sequence (Gallagher *et al.*, 1997). Because ANK repeats form protein-binding sites using multiple repeats, deletion of individual repeats by alternative splicing has the potential to produce novel binding sites analogous to V(D)J joining in immunoglobulin genes (reviewed in Grawunder *et al.*, 1998).

A second distinctive feature of the ANK repeats of D34 is the curvature of the repeat stack. ANK repeat stacks of different proteins have unique curvatures that presumably are adapted to associate best with specific protein ligands. Comparison of r.m.s. deviations between individual repeats of several proteins shows that curvature is not controlled by variations in the orientation of the two helices (Venkataramani *et al.*, 1998; data not shown). Instead, the relative side chain volumes of residues that form the helical bundle cores of adjacent repeats determine the geometric parameters of the curvature. Because the repeats of D34 are highly similar, the contribution of individual residues within the helical core can be assessed for their effect on curvature. Examination of core residues suggests that the relative side chain volumes of residues at positions 10, 17 and 18 largely determine the curvature of

the repeat stack, with position 10 playing a central role. Normally, this position contains alanine or, to a lesser extent, serine or cysteine. When larger aliphatic residues occupy position 10, the curvature of both the ankyrin groove surface and the bottom surface is reduced. An example of this effect can be seen at the interface between repeats 18 and 19 in D34, which features a valine (Val577) at position 10 in repeat 18. Similar curvature flattening can be observed in myotrophin, p19INK4D, bcl-3, pap- β , 53BP and I κ B α (Gorina and Pavletich, 1996; Baumgartner *et al.*, 1998; Huxford *et al.*, 1998; Jacobs and Harrison, 1998; Yang *et al.*, 1998; Mandiyan *et al.*, 1999; Michel *et al.*, 2001). Substitutions at positions 17 and 18 also affect curvature, though to a lesser extent than at position 10. Usually, positions 17 and 18 harbor mid-sized valines and threonines, which, in conjunction with a small residue at position 10, produce concave curvature in both the ankyrin groove and bottom surfaces. In the D34 structure, we observe seven deviations from mid-sized residues at positions 17 and 18. Six of these deviations are compensatory such that alanines at position 18 pack against larger aliphatics at position 17 in the following repeat. An example of larger residues increasing curvature about the ankyrin groove is seen at the interface between repeats 22 and 23. In this way, core residues at positions 10, 17 and 18 modulate the topology of the repeat stack and thereby position solvent-exposed residues for associations with specific protein targets.

Binding interactions

ANK repeats associate with a wide variety of protein sequences through contact residues that can be presented on any surface of the repeat stack. High resolution structures have been determined for three protein complexes involving ANK repeat proteins: INK4 inhibitors and CDK6; GABP β and GABP α ; and I κ B α and NF- κ B (Batchelor *et al.*, 1998; Brotherton *et al.*, 1998; Huxford *et al.*, 1998; Jacobs and Harrison, 1998; Russo *et al.*, 1998). Each association is distinct and involves residues on the end (I κ B α), top (I κ B α), bottom (INK4) and ankyrin groove surfaces (I κ B α , INK4 and GABP β). Additionally, the back surface has been observed to form intramolecular contacts in the SWI6 and PAP β structures and may participate in the intermolecular contacts of some ANK repeat associations (Foord *et al.*, 1999; Mandiyan *et al.*, 1999).

The ankyrin groove surface may be a frequent site of protein interaction for several reasons. First, this surface contains many variable residues that presumably are important for binding site specificity. Secondly, this surface has the broadest range of curvature variation. Finally, the ankyrin groove appears to be capable of interacting with a wide variety of protein secondary structural elements including loops (GABP β), β -sheets (INK4), helices (I κ B α) and extended strands (D34).

In the D34 structure, the ankyrin groove surface of repeats 20–24 provides the binding site for a portion of the spectrin-binding domain. The nature and extent of this contact suggest that it may fix the orientation of the entire spectrin-binding domain relative to the ANK repeats. This may help direct spectrin-binding activity away from the membrane surface. A fixed orientation may also facilitate the association of ankyrin with the Na/K ATPase because

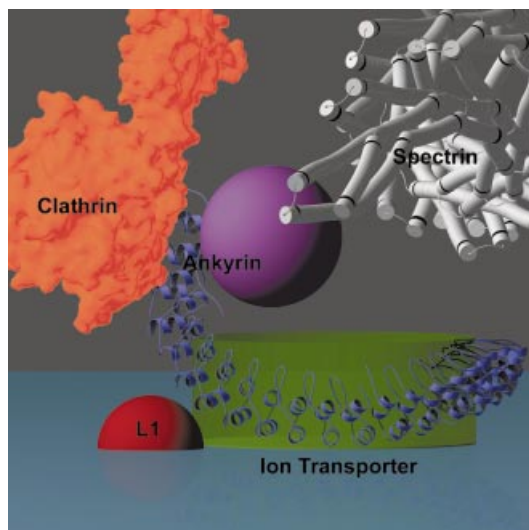


Fig. 7. Model of ankyrin function. A model for the molecular organization of ankyrin and its binding partners at the membrane. Ankyrin is colored purple with its membrane-binding domain depicted as a ribbon. This domain wraps around an ion transporter shown as a transparent green cylinder protruding from the cytoplasmic surface of the membrane (light blue). The cytoplasmic domain of an L1 cell adhesion molecule is shown as a red half sphere near the back surface of repeats 18 and 19 of the membrane-binding domain. The spectrin-binding domain of ankyrin is depicted as a purple sphere connected to the C-terminal end of the membrane-binding domain. Spectrin is shown end-on in a white rod representation. Clathrin heavy chain is shown in an orange space-filling representation.

high affinity binding requires both membrane-binding and spectrin-binding domains (Davis and Bennett, 1990; Thevananther *et al.*, 1998).

Our modeling predicts that the ankyrin groove and bottom surfaces of D34 mediate the association with CDB3. This model is consistent with a number of features of the ankyrinR–anion exchanger interaction reported in the literature. Normally, the anion exchanger exists as a dimer in the membrane. Binding of ankyrinR brings together two dimers to form a tetramer (Che *et al.*, 1997). *In vitro* binding assays have shown that the ANK repeats assemble CDB3 tetramers using two cooperatively linked sites of interaction for the CDB3 dimer. One dimer interacts with site one in the D2 region (repeats 7–12), while a second dimer interacts with site two in the D34 region (Michaely and Bennett, 1995a). The N-terminus of CDB3 appears to be required for both the D2 and D34 interactions (Wang *et al.*, 1995). Our proposed model predicts extensive contacts between a surface containing the N-terminal region of CDB3 and both the bottom and ankyrin groove surfaces of D34. The β -hairpins of D34 fit into a groove formed at the dimer–dimer interface of the CDB3 tetramer. The D2 region is directed toward the N-terminus of the distal subunit in the second dimer. This model predicts that the positive cooperativity observed in the binding of the CDB3 dimers derives from a stabilization of the anion exchanger tetramer through a contiguous series of interactions that span >12 repeats.

A proposal for the molecular basis of ankyrin function

The D34 region of ankyrins can associate with ion transporters, cell adhesion molecules and clathrin. Ion

transporters represent the largest class of ankyrin-binding proteins. These associations appear to employ a common surface because CDB3 can compete with ankyrin binding to most sites in brain membranes and competes directly with ankyrin binding to Na/K ATPase and voltage-gated Na channels (Davis and Bennett, 1986, 1990; Srinivasan *et al.*, 1988). Our model for the CDB3 interaction predicts that the 24 ANK repeats of the membrane-binding domain wrap around the CDB3 tetramer, with the bottom and ankyrin groove surfaces directed toward the tetramer surface. We propose that these surfaces are primarily responsible for interactions with ion transporters. In contrast, CDB3 is unable to compete with either L1 cell adhesion molecules or clathrin (Michaely and Bennett, 1995b; Figure 4), suggesting that these proteins bind distinct surfaces on the ANK repeats. Our models predict that clathrin associates with the top surface, distal to the CDB3 site. This region is expected to be farthest from the membrane surface, oriented toward the cytosol and in position to associate with the clathrin lattice. L1 cell adhesion molecules associate with a surface that involves both repeats 13–18 and repeats 19–24 (Michaely and Bennett, 1995b). Based upon the model for the CDB3 association, L1 molecules may associate with the top and/or back surfaces near repeats 18 and 19. Figure 7 depicts a potential arrangement of the molecular organization of ankyrin and its binding partners. This model is the first to provide a structural framework for ankyrin-directed integration of cellular function.

Materials and methods

Crystal structure determination

cDNA encoding residues 402–827 of ankyrinR (D34) was synthesized by PCR and ligated into the pGEX kg GST expression vector (Amersham Biosystems) using the *EcoRI* and *HindIII* restriction sites. The resulting plasmid was then transformed into the DE3 strain of *Escherichia coli*. After expression, the D34–GST fusion was bound to glutathione–agarose, eluted by thrombin cleavage and purified to homogeneity by size exclusion chromatography on Superdex 75 (Amersham Biosystems) in buffer A (20 mM HEPES/Na pH 7.5, 500 mM NaBr, 1 mM EDTA and 1 mM DTT). The SeMet variant of D34 was expressed in the methionine-auxotrophic *E. coli* strain, B834, grown in minimal medium supplemented with the natural amino acids and SeMet. Expression and purification behavior were unchanged.

Crystals of D34 were obtained at 4°C by the vapor diffusion method from drops containing 1 μ l of protein (25 mg/ml in buffer A) plus 1 μ l of reservoir solution [100 mM HEPES pH 7.5, 500 mM CaCl₂, 7–10% (v/v) PEG400 and 5% (v/v) acetonitrile] equilibrated against 1 ml of reservoir solution. Hexagonal crystals appeared after 2 days and grew to a maximum size of 1.0 \times 0.4 mm within 5 days. Crystallization of the seleno-methionine variant was achieved under similar conditions with a protein concentration of 20 mg/ml and a reservoir solution that consisted of 100 mM HEPES/Na pH 7.5, 300 mM CaCl₂, 2–5% (v/v) PEG400 and 9–11% (v/v) acetonitrile. Crystals exhibited symmetry of space group *P*6₃22 with cell dimensions of $a = b = 138$ Å, $c = 197$ Å and one molecule in the asymmetric unit (80% solvent content). Prior to data collection, native crystals were transferred at 4°C into harvesting solution [100 mM HEPES pH 7.5, 500 mM CaCl₂, 10% (v/v) PEG400, 5% (v/v) acetonitrile and 250 mM NaBr]. For cryo-protection, the concentration of PEG400 was increased in 5% increments every 30 min to a final concentration of 30% (v/v). SeMet crystals were treated similarly except that the harvesting solution consisted of 100 mM HEPES pH 7.5, 300 mM CaCl₂, 2.5% (v/v) PEG400, 9% (v/v) acetonitrile and 250 mM NaBr. Crystals were then flash-cooled in liquid propane.

The native crystals diffracted anisotropically to a maximum Bragg spacing (d_{\min}) of 2.5 Å and isotropically to a d_{\min} of 2.7 Å when exposed to synchrotron radiation. The average diffraction intensity is relatively strong to a d_{\min} of 4 Å, but suffers a dramatic decrease to the high

resolution limit. The structure was solved by the MAD method using the SeMet variant. The MAD experiment was carried out at beamline 19-ID (SBC-CAT) at the Advanced Photon Source (Argonne National Laboratory, Argonne, IL). One data set was collected at the peak energy of the selenium K-edge absorption, and a second was collected at the inflection point energy. Data were indexed, integrated and scaled with the HKL2000 program package (Otwinowski and Minor, 1997). Intensities were converted to structure factor amplitudes and placed on an approximate absolute scale by the program TRUNCATE from the CCP4 package (French and Wilson, 1978; CCP4, 1994). Eight selenium sites were identified from the peak energy data set using the Patterson search routine in the program package CNS 1.0 (Brünger *et al.*, 1998). Phases were calculated and refined using both SeMet data sets in the program MLPHARE (Otwinowski, 1991), resulting in an overall figure of merit of 0.24 for data between 35.0 and 2.8 Å. The resulting phases were improved further by density modification with histogram matching in the program DM (Cowtan and Main, 1998), resulting in a final overall figure of merit of 0.57. Data collection and MAD phasing statistics are shown in Table I.

Model building and structure refinement

Inspection of electron density maps and model building were performed in the program O (Jones *et al.*, 1991). Refinement of the structure was carried out in the program package CNS 1.0 with a random 3.7% subset of all data set aside for an R_{free} calculation. Several cycles of simulated annealing, conjugate gradient minimization and calculation of individual atomic displacement parameters (ADPs) using data between 20.0 and 3.5 Å, coupled with model building allowed for the construction of a complete model for residues 405–797 and 802–812. Calculation of overall anisotropic ADPs and bulk solvent correction were used throughout. Subsequent cycles of standard positional refinement and individual isotropic ADP refinement coupled with cycles of model rebuilding were carried out against all data between 30.0 and 2.7 Å. Halide ions were added where stereochemically reasonable after the protein model was complete. Due to the low resolution of the data set and the high concentration of bromides and chlorides in the crystallization and freezing solutions, these atoms were assigned as halides rather than waters. The average isotropic ADP for these atoms is similar to the values for the protein. Overall, the N-terminal half of the structure is less well ordered than the C-terminal half, as reflected in the higher ADPs for this region. The final model contains residues 405–797, 802–812, one bromide ion and nine chloride ions. The R_{free} value is 30.3% and the R_{work} value is 31.9% (see Table I).

Docking simulations

Potential modes for the binding of D34 to CDB3 (Zhang *et al.*, 2000) and the CTD (ter Haar *et al.*, 1998) were calculated with the program package FT-DOCK using default parameters (Gabb *et al.*, 1997). Briefly, one of the binding partners was treated as the 'static' molecule, while the other was treated as the 'mobile' molecule whose position was varied to generate possible docking modes. We reduced an initial list of 10 000 potential solutions by eliminating models that were not compatible with biochemical data or that led to steric conflicts.

For modeling of the D34–CDB3 complex, D34 was treated as the 'static' molecule, while a monomer of CDB3 was used as the 'mobile' molecule. Only 32 potential solutions were compatible with mutagenesis and biochemical studies (Davis *et al.*, 1989, 1991; Willardson *et al.*, 1989; Michaely and Bennett, 1995a). The top seven and a total of 27 of the 32 models place CDB3 on the bottom surface.

For modeling of the D34–CTD complex, the CTD was treated as the 'static' molecule, while repeats 19–24 (region D4, residues 600–812) of D34 were used as the 'mobile' molecule. All solutions were eliminated that involved the α -helical segment of the CTD or that led to steric conflicts with repeats 13–18. Models were then screened for modes that involved residues 1–14 of the CTD and did not conflict with the proposed CDB3-binding site.

Immunoblotting

Ankyrin constructs were chromatographed on 5–17% linear gradient SDS–polyacrylamide gels and transferred to nylon membranes. Membranes were blocked with buffer B (10 mM HEPES pH 7.5, 100 mM NaCl, 1 mM EDTA, 1 mM DTT, 0.1% Tween-20 and 5 mg/ml bovine serum albumin) and then incubated overnight at 4°C with various regions of the CTD fused to GST in buffer B. Membranes were then washed five times with buffer B and twice with buffer C (10 mM HEPES pH 7.5, 100 mM NaCl, 1 mM EDTA), followed by incubation for 15 min on ice with 3% paraformaldehyde in buffer C. The membranes were next

washed three times with buffer C and processed using standard immunoblotting techniques with a monoclonal antibody against GST (Santa Cruz), horseradish peroxidase-conjugated secondary antibodies (Bio-Rad) and enhanced chemiluminescence (ECL) detection (Amersham Biosystems).

Figure preparation

Unless otherwise indicated in the figure legends, all images were composed with BOBSCRIPT (2.4) (Esnouf, 1999) and rendered with POVray (3.0.2) (<http://povray.org/>). GLR (0.7) was used to facilitate the figure preparation (L.Esser, personal communication).

PDB accession code

The coordinates for the D34 structure have been deposited in the Protein Data Bank under accession code 1N11. Coordinates for modeled complexes are available upon request.

Acknowledgements

We would like to thank Sandra Hill for her valuable technical assistance and Brenda Pallares for administrative assistance. The authors are also grateful for the expert aid in data collection provided by Andrzej Joachimiak and the staff of the Structural Biology 19-ID beamline. Use of the Argonne National Laboratory Structural Biology Center beamlines at the Advanced Photon Source was supported by the US Department of Energy, Office of Biological and Environmental Research, under contract No. W-31-109-ENG-38. This work was supported by grants from the National Institutes of Health, HL 20948, GM 52016 and the Perot Family Foundation.

References

- Aurora,R. and Rose,G.D. (1998) Helix capping. *Protein Sci.*, **7**, 21–38.
- Batchelor,A.H., Piper,D.E., de la Brousse,F.C., McKnight,S.L., Wolberger,C., Yang,Y., Nanduri,S., Sen,S. and Qin,J. (1998) The structure of GABP α/β : an ETS domain–ankyrin repeat heterodimer bound to DNA. *Science*, **279**, 1037–1041.
- Baumgartner,R., Fernandez-Catalan,C., Winoto,A., Huber,R., Engh,R.A. and Holak,T.A. (1998) Structure of human cyclin-dependent kinase inhibitor p19INK4d: comparison to known ankyrin-repeat-containing structures and implications for the dysfunction of tumor suppressor p16INK4a. *Structure*, **6**, 1279–1290.
- Bennett,V. and Baines,A.J. (2001) Spectrin and ankyrin-based pathways: metazoan inventions for integrating cells into tissues. *Physiol. Rev.*, **81**, 1353–1392.
- Bennett,V. and Stenbuck,P.J. (1979) The membrane attachment protein for spectrin is associated with band 3 in human erythrocyte membranes. *Nature*, **280**, 468–473.
- Bourguignon,L.Y., Chu,A., Jin,H. and Brandt,N.R. (1995) Ryanodine receptor–ankyrin interaction regulates internal Ca²⁺ release in mouse T-lymphoma cells. *J. Biol. Chem.*, **270**, 17917–17922.
- Brotherton,D.H. *et al.* (1998) Crystal structure of the complex of the cyclin D-dependent kinase Cdk6 bound to the cell-cycle inhibitor p19INK4d. *Nature*, **395**, 244–250.
- Brünger,A.T. *et al.* (1998) Crystallography and NMR system: a new software suite for macromolecular structure determination. *Acta Crystallogr. D*, **54**, 905–921.
- Che,A., Morrison,I.E., Pan,R. and Cherry,R.J. (1997) Restriction by ankyrin of band 3 rotational mobility in human erythrocyte membranes and reconstituted lipid vesicles. *Biochemistry*, **36**, 9588–9595.
- CCP4 (1994) The CCP4 suite: programs for protein crystallography. *Acta Crystallogr. D*, **50**, 760–763.
- Cowtan,K. and Main,P. (1998) Miscellaneous algorithms for density modification. *Acta Crystallogr. D*, **54**, 487–493.
- Davis,J.Q. and Bennett,V. (1986) Association of brain ankyrin with brain membranes and isolation of active proteolytic fragments of membrane-associated ankyrin-binding protein(s). *J. Biol. Chem.*, **261**, 16198–16206.
- Davis,J.Q. and Bennett,V. (1990) The anion exchanger and Na⁺K⁺-ATPase interact with distinct sites on ankyrin in *in vitro* assays. *J. Biol. Chem.*, **265**, 17252–17256.
- Davis,J.Q., McLaughlin,T. and Bennett,V. (1993) Ankyrin-binding proteins related to nervous system cell adhesion molecules:

- candidates to provide transmembrane and intercellular connections in adult brain. *J. Cell Biol.*, **121**, 121–133.
- Davis, L., Lux, S.E. and Bennett, V. (1989) Mapping the ankyrin-binding site of the human erythrocyte anion exchanger. *J. Biol. Chem.*, **264**, 9665–9672.
- Davis, L.H., Otto, E. and Bennett, V. (1991) Specific 33-residue repeat(s) of erythrocyte ankyrin associate with the anion exchanger. *J. Biol. Chem.*, **266**, 11163–11169.
- Edwards, M.S., Sternberg, J.E. and Thornton, J.M. (1987) Structural and sequence patterns in the loops of $\beta\alpha\beta$ units. *Protein Eng.*, **1**, 173–181.
- Esnouf, R. (1999) Further additions to MolScript version 1.4, including reading and contouring of electron-density maps. *Acta Crystallogr. D*, **55**, 938–940.
- Festy, F., Robert, J.C., Bresseur, R. and Thomas, A. (2001) Interaction between the N-terminal domain of gastric H,K-ATPase and the spectrin binding domain of ankyrin III. *J. Biol. Chem.*, **276**, 7721–7726.
- Foord, R. et al. (1999) X-ray structural analysis of the yeast cell cycle regulator Swi6 reveals variations of the ankyrin fold and has implications for Swi6 function. *Nat. Struct. Biol.*, **6**, 157–165.
- French, G.S. and Wilson, K.S. (1978) On the treatment of negative intensity observations. *Acta Crystallogr. A*, **34**, 517–525.
- Gabb, H.A., Jackson, R.M. and Sternberg, M.J. (1997) Modelling protein docking using shape complementarity, electrostatics and biochemical information. *J. Mol. Biol.*, **272**, 106–120.
- Gallagher, P.G., Tse, W.T., Scarpa, A.L., Lux, S.E. and Forget, B.G. (1997) Structure and organization of the human ankyrin-1 gene. Basis for complexity of pre-mRNA processing. *J. Biol. Chem.*, **272**, 19220–19228.
- Gorina, S. and Pavletich, N.P. (1996) Structure of the p53 tumor suppressor bound to the ankyrin and SH3 domains of 53BP2. *Science*, **274**, 1001–1005.
- Grawunder, U., West, R.B. and Lieber, M.R. (1998) Antigen receptor gene rearrangement. *Curr. Opin. Immunol.*, **10**, 172–180.
- Hortsch, M., Homer, D., Malhotra, J.D., Chang, S., Frankel, J., Jefford, G. and Dubreuil, R.R. (1998) Structural requirements for outside-in and inside-out signaling by *Drosophila* neuroglian, a member of the L1 family of cell adhesion molecules. *J. Cell Biol.*, **142**, 251–261.
- Huxford, T., Huang, D.B., Malek, S. and Ghosh, G. (1998) The crystal structure of the I κ B α /NF- κ B complex reveals mechanisms of NF- κ B inactivation. *Cell*, **95**, 759–770.
- Jacobs, M.D. and Harrison, S.C. (1998) Structure of an I κ B α /NF κ B complex. *Cell*, **95**, 749–758.
- Jones, T.A., Zou, J.Y., Cowan, S.W. and Kjeldgaard, M. (1991) Improved methods for building protein models in electron density maps and the location of errors in these models. *Acta Crystallogr. A*, **47**, 110–119.
- Joseph, S.K. and Samanta, S. (1993) Detergent solubility of the inositol trisphosphate receptor in rat brain membranes. Evidence for association of the receptor with ankyrin. *J. Biol. Chem.*, **268**, 6477–6486.
- Li, Z.P., Burke, E.P., Frank, J.S., Bennett, V. and Philipson, K.D. (1993) The cardiac Na⁺-Ca²⁺ exchanger binds to the cytoskeletal protein ankyrin. *J. Biol. Chem.*, **268**, 11489–11491.
- Mandiyani, V., Andreev, J., Schlessinger, J. and Hubbard, S.R. (1999) Crystal structure of the ARF-GAP domain and ankyrin repeats of PYK2-associated protein β . *EMBO J.*, **18**, 6890–6898.
- Michaely, P. and Bennett, V. (1993) The membrane-binding domain of ankyrin contains four independently folded subdomains, each comprised of six ankyrin repeats. *J. Biol. Chem.*, **268**, 22703–22709.
- Michaely, P. and Bennett, V. (1995a) The ANK repeats of erythrocyte ankyrin form two distinct but cooperative binding sites for the erythrocyte anion exchanger. *J. Biol. Chem.*, **270**, 22050–22057.
- Michaely, P. and Bennett, V. (1995b) Mechanism for binding site diversity on ankyrin. Comparison of binding sites on ankyrin for neurofascin and the Cl⁻/HCO₃⁻ anion exchanger. *J. Biol. Chem.*, **270**, 31298–31302.
- Michaely, P., Kamal, A., Anderson, R.G. and Bennett, V. (1999) A requirement for ankyrin binding to clathrin during coated pit budding. *J. Biol. Chem.*, **274**, 35908–35913.
- Michel, F., Soler-Lopez, M., Petosa, C., Cramer, P., Siebenlist, U. and Muller, C.W. (2001) Crystal structure of the ankyrin repeat domain of Bcl-3: a unique member of the I κ B protein family. *EMBO J.*, **20**, 6180–6190.
- More, M.I., Kirsch, F.P. and Rathjen, F.G. (2001) Targeted ablation of NrCAM or ankyrin-B results in disorganized lens fibers leading to cataract formation. *J. Cell Biol.*, **154**, 187–196.
- Nelson, W.J. and Veshnock, P.J. (1987) Ankyrin binding to (Na⁺ + K⁺)ATPase and implications for the organization of membrane domains in polarized cells. *Nature*, **328**, 533–536.
- Nicholls, A., Sharp, K.A. and Honig, B. (1991) Protein folding and association: insights from the interfacial and thermodynamic properties of hydrocarbons. *Proteins*, **11**, 281–296.
- Otwinowski, Z. (1991) Maximum likelihood refinement of heavy atom parameters. In Wolf, W., Evans, P.R. and Leslie, A.G.W. (eds), *Isomorphous Replacement and Anomalous Scattering*. Science & Engineering Research Council, Cambridge, UK, pp. 80–86.
- Otwinowski, Z. and Minor, W. (1997) Processing of X-ray diffraction data collected in oscillation mode. *Methods Enzymol.*, **276**, 307–326.
- Richardson, J.S. and Richardson, D.C. (1988) Amino acid preferences for specific locations at the ends of α helices. *Science*, **240**, 1648–1652.
- Russo, A.A., Tong, L., Lee, J.O., Jeffrey, P.D. and Pavletich, N.P. (1998) Structural basis for inhibition of the cyclin-dependent kinase Cdk6 by the tumour suppressor p16INK4a. *Nature*, **395**, 237–243.
- Sedgwick, S.G. and Smerdon, S.J. (1999) The ankyrin repeat: a diversity of interactions on a common structural framework. *Trends Biochem. Sci.*, **24**, 311–316.
- Shoemaker, K.R., Kim, P.S., York, E.J., Stewart, J.M. and Baldwin, R.L. (1987) Tests of the helix dipole model for stabilization of α -helices. *Nature*, **326**, 563–567.
- Srinivasan, Y., Elmer, L., Davis, J., Bennett, V. and Angelides, K. (1988) Ankyrin and spectrin associate with voltage-dependent sodium channels in brain. *Nature*, **333**, 177–180.
- Srinivasan, Y., Lewallen, M. and Angelides, K.J. (1992) Mapping the binding site on ankyrin for the voltage-dependent sodium channel from brain. *J. Biol. Chem.*, **267**, 7483–7489.
- ter Haar, E., Musacchio, A., Harrison, S.C. and Kirchhausen, T. (1998) Atomic structure of clathrin: a β propeller terminal domain joins an α zigzag linker. *Cell*, **95**, 563–573.
- Thevananther, S., Kolli, A.H. and Devarajan, P. (1998) Identification of a novel ankyrin isoform (AnkG190) in kidney and lung that associates with the plasma membrane and binds α -Na, K-ATPase. *J. Biol. Chem.*, **273**, 23952–23958.
- Tuvia, S., Buhusi, M., Davis, L., Reedy, M. and Bennett, V. (1999) Ankyrin-B is required for intracellular sorting of structurally diverse Ca²⁺ homeostasis proteins. *J. Cell Biol.*, **147**, 995–1008.
- Venkataramani, R., Swaminathan, K. and Marmorstein, R. (1998) Crystal structure of the CDK4/6 inhibitory protein p18INK4c provides insights into ankyrin-like repeat structure/function and tumor-derived p16INK4 mutations. *Nat. Struct. Biol.*, **5**, 74–81.
- Wang, C.C., Moriyama, R., Lombardo, C.R. and Low, P.S. (1995) Partial characterization of the cytoplasmic domain of human kidney band 3. *J. Biol. Chem.*, **270**, 17892–17897.
- Willardson, B.M., Thevenin, B.J., Harrison, M.L., Kuster, W.M., Benson, M.D. and Low, P.S. (1989) Localization of the ankyrin-binding site on erythrocyte membrane protein, band 3. *J. Biol. Chem.*, **264**, 15893–15899.
- Yang, Y., Nanduri, S., Sen, S. and Qin, J. (1998) The structural basis of ankyrin-like repeat function as revealed by the solution structure of myotrophin. *Structure*, **6**, 619–626.
- Zhang, D., Kiyatkin, A., Bolin, J.T. and Low, P.S. (2000) Crystallographic structure and functional interpretation of the cytoplasmic domain of erythrocyte membrane band 3. *Blood*, **96**, 2925–2933.

Received July 25, 2002; revised October 14, 2002;
accepted October 17, 2002